Comparison of breast ductal branching pattern classification using x-ray galactograms and MR autogalactograms

Predrag R. Bakic*, Mark A. Rosen, Andrew D.A. Maidment
Department of Radiology, University of Pennsylvania, 3400 Spruce St., Philadelphia, PA 19104

ABSTRACT

We have analyzed the branching patterns of the breast ductal network visible in magnetic resonance (MR) autogalactograms – images of breast ducts which appear enhanced due to the presence of proteinacous or hemorrhagic material in the ducts. The enhanced portions of the ductal network were segmented separately in MRI slices acquired with a 3D GRASS sequence. A semi-automated region growing algorithm was used for segmentation. The ductal network was manually constructed from the segmented portions in each slice. The branching pattern was analyzed by calculating ramification (R-) matrices, whose elements represent the probabilities of branching at various levels of a ductal tree. The R-matrix elements have been used to classify the analyzed cases into those with and without radiological findings. The classification accuracy was estimated using the radiologists' reports as ground truth. An ROC analysis was performed to assess the classification accuracy. The classification of nine MR autogalactograms from eight women yielded an area under the ROC curve of A=0.73. This performance is comparable with our previous analysis of 25 2D x-ray galactograms from 15 women (A=0.88). The observed results support our hypothesis that a relationship exists between the topological properties of the breast ductal network and the underlying breast pathology.

Keywords: Breast cancer, breast ducts, galactography, autogalactograms, ramification matrices, ROC analysis.

1. INTRODUCTION

The glandular portion of the breast consists of a network of lactiferous ducts. Breast ducts propagate from the nipple toward the chest wall in a branching network, ending in glandular lobuli which produce milk during lactation. It is known that about 90% of breast cancers arise in the ductal epithelium[1]. The initial spread of cancer is also observed to follow the ductal pathways, as indicated by the spatial morphology of calcification clusters[2].

Our motivation for the analysis of breast ductal topology began with our work on 3D breast tissue simulation for the purpose of generating synthetic mammograms[3, 4]. Such synthetic images have been used in analysis of parenchymal pattern[5], tissue specific dosimetry in mammography[6, 7], evaluation of mammogram registration methods[8], and evaluation of wavelet-based mammogram processing techniques[9].

We hypothesize that the topological properties of the breast ductal network are correlated with the developmental stage and pathological state of the breast tissue. This hypothesis is supported by the results of animal experiments, analysis of mammographic parenchymal patterns, and our own results in classification of galactograms. In a study of murine ductal networks, Atwood *et al.*[10] observed significant differences in the number of branch points and ductal length in mice treated in vivo with progesterone and estrogen, compared to normal controls. In addition, Bonta *et al.*[11] achieved an improved prognosis of axillary lymph node status by combining features extracted from mammographic masses with the features from contralateral normal parenchyma, thus implying systemic effects of breast cancer.

In our previous study, we analyzed ductal branching patterns identified from clinical x-ray galactograms, 2D contrast-enhanced images of the ductal network[12]. Galactography is a clinical procedure for imaging the contrast–enhanced ductal network in women with nipple discharge and no palpable or mammographic lesions[13]. It is performed by carefully identifying the discharging nipple orifice, introducing a blunt needle, and injecting a small amount of iodine-based radiographic contrast material. Pre- and post-contrast mammograms are obtained with the needle in place, thereby revealing the breast lobe that contains the discharging duct. Various ductal patterns (e.g., filling defects, ductal ectasia)

* Predrag.Bakic@uphs.upenn.edu; Phone: 215 746 8758; Fax: 215 746 8764

Medical Imaging 2006: Image Processing, edited by Joseph M. Reinhardt, Josien P. W. Pluim,
Proc. of SPIE Vol. 6144, 614425, (2006) · 0277-786X/06/$15 · doi: 10.1117/12.654731

can be recognized from galactograms[14]. Galactography lacks specificity[1], and thus results in a large number of biopsies with normal or benign results. A part of our original motivation for the analysis of ductal morphology was to investigate a classification method for galactograms, which might help reduce the number of biopsies with negative results and the related psychological and economic effects.

We have performed classification of galactograms based on the ductal topology using ramification (R-)matrices[12]. The elements of an R-matrix represent the probability of branching at various levels of a ramified tree[15]. We used selected R-matrix elements to classify galactograms into cases with radiological findings and normal cases. To reconstruct the ductal topology, first, each branch in the ductal network was manually traced on a sheet of tracing paper placed over the galactogram attached to a light box. Next, the points where ducts branched were distinguished from the points of overlap based on the assumption that the latter are brighter, due to the increased x-ray attenuation. Large ducts were reconstructed by connecting the marked points. In each segmented ductal tree, we identified the root, internal and terminal nodes, and branches. These tree elements were then appropriately labeled, in order to compute the branching probabilities as described in Section 2.2.

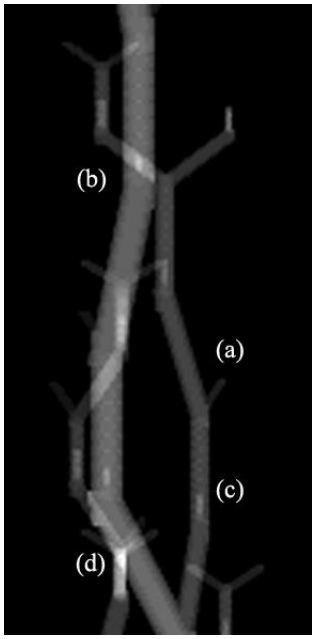

This segmentation approach is sensitive to the orientation of the plane in which the ducts branch or overlap (see Figure 1). This is the result of the 2D projective nature of galactography. As a consequence, we have attempted to analyze ductal branching using 3D magnetic resonance (MR) images of the breast. MR imaging has been reported as a potential alternative to galactography[16]. Acquisition of true contrast-enhanced MR galactograms, with the injection of MR contrast material into a breast ductal lobe, is not performed at our institution. Instead, we have chosen to study the breast ductal branching patterns in MR autogalactograms. We have coined the term "autogalactogram" to refer to MR images with enhancement of the ductal network caused by the presence of protein or blood in the ducts. In this paper we describe our results in classification of MR autogalactograms using the R-matrices.

Figure 1: A portion of a simulated contrast-enhanced galactogram, illustrating problems encountered while tracing the ductal tree. The point where ducts overlap (a) appears brighter than the point of branching (b), except when the orientation of the plane in which the duct branches significantly differs from the image plane (c), or when there are many ducts overlapping at the same point (d).

2. METHODOLOGY

2.1 Acquisition and segmentation of MR autogalactograms

The MR images used in this study were acquired at the Hospital of the University of Pennsylvania. One MR pulse sequence was selected for analysis based upon the conspicuity of the ductal self-enhancement. The preferred MR sequence was the 3D slab inter-leaved spoiled gradient-echo sequence (GRASS) with intermittent fat-selective partial inversion for fat suppression[16]. In this acquisition protocol, each breast is imaged under gentle compression using exactly 28 slices; the slice thickness varied as a result. The field-of-view varied from 16 to 18 cm depending upon the breast size, with a resolution of 512×512 pixels. This pulse sequence was applied before and after intravenous administration of a contrast agent. We used the pre-contrast images for tracing the ductal network. In some instances, we consulted the post-contrast images to confirm the segmentation of the proteinaceous and hemorrhagic material, since the signal intensity of this material should not change between pre- and post-contrast images.

The self-enhanced regions of the ductal network were segmented separately in individual MR images (slices). This segmentation was performed using a region growing algorithm selected from the ITK library[17]. For each ductal region visible in an MR slice, a seed pixel was selected manually and used as input to the region growing algorithm. Parameters of the algorithm were adjusted interactively, based upon visual comparison of the segmentation results with the original image. The ductal trees were reconstructed manually using weighted sums of segmented regions within

consecutive slice pairs. In a few cases with a large number of very small enhanced regions, we performed segmentation by thresholding the MR slices. The threshold was selected using an initial region-growing based segmentation, applied initially to 2-3 MR slices per breast. A histogram of MR intensities within the regions segmented using this initial threshold was calculated and the final threshold value was selected. The final threshold value was determined by considering the trade-off between the area of the erroneously segmented regions outside of the visible self-enhanced ductal portions and the degree of thinning the segmented ductal portions. The ductal network was, then, manually reconstructed from the segmented regions in all MR slices, as above, using weighted sums of adjacent slices. The R matrices corresponding to the segmented ductal trees were computed using the approach described in the next section.

2.2 Computing the probabilities of ductal branching using ramification (R-) matrices

R-matrix elements represent the probability of branching at various levels of a ramified tree. In order to compute these probabilities for a segmented ductal tree, we have labeled the root, internal and terminal nodes, and branches, as described by Viennot *et al.*[15]: (a) All terminal branches have label 1; (b) A "parent" branch whose "children" have labels i and j will be labeled by max(i, j) if $i \neq j$, or by (i + 1) if i = j; (c) The labeling procedure continues until the root branch is reached. The label of the root branch, s, is called the Strahler number of the tree structure. The R matrix of a tree with Strahler number s is a lower triangular matrix, defined as:

$$\mathbf{R}_{(s-1),s}=\left[r_{k,j}=b_{k,j}/a_k, k\in(2,s), j\in(1,k)\right], \quad (1)$$

where a_k is equal to the number of branches with label k. For $j\neq k$, $b_{k,j}$ is the number of pairs of branches with labels k and j, while for $j=k$, $b_{k,j}$ is the number of pairs of branches both labeled k-1 descending from a node. Therefore, $r_{k,j}=b_{k,j}/a_k=p(b_{k,j}|a_k)$ is the probability that a branch with label k will bifurcate into branches with the appropriate labels. As an example, Figure 2h shows the numerically labeled branches of the segmented ductal tree from case #4; the corresponding R-matrix is given by Equation 2.

2.3 Classification of ductal trees

We selected R-matrix element $r_{2,2}$ as the feature to be used for classification of MR autogalactograms. This selection was based on our previous study of x-ray galactograms, in which we used R-matrix elements and a Bayesian decision rule to determine the optimal classification threshold[12]. In that study, we assumed a normal distribution of the features with equal standard deviations for both classes. Classification performance was evaluated using the leave-one-out (jackknife) method[18]. Using that approach[12], we observed the best classification accuracy for R-matrix element $r_{3,3}$. All R-matrices used in the galactography study had a Strahler number of s=4. In the autogalactography study, we used R-matrices with a Strahler number of s=3. It can be shown that element $r_{3,3}$ of a R-matrix with s=4 corresponds to element $r_{2,2}$ of a tree with s=3.

The classification of ductal trees reconstructed from x-ray galactograms and MR autogalactograms were compared using ROC curves. The estimate of the area under the ROC curve was generated using the Wilcoxon method[19]. Initially, we compared performance by analyzing images individually. We also analyzed classification of patients, taking into account that some patients had several images available. Three strategies were considered. First, a *conservative* strategy of assigning the *maximum* feature value from the individual images as the single feature value of the case. Second, a *followup* strategy of assigning the *minimum* feature value from the individual images. Third, a *majority vote* approach of assigning the *average* feature value from individual images to the case. Note that in our previously published analysis of x-ray galactograms, we performed only the classification of individual galactograms.

3. DATA

Forty–six women with autogalactograms were identified retrospectively with the help of a MR radiologist after searching through the MR reports for words "protein", "blood", "proteinaceous", and "hemorrhagic". The MR studies occurred between August 1998 and April 2005 at the Hospital of the University of Pennsylvania. The MR images were available for 23 of the 46 women. Of the available cases, we excluded 13 in which the ductal branching was not sufficiently conspicuous. Of the remaining 10 women with visible ducts, we reconstructed eleven ductal trees; two individual ductal lobes were visible in one image set. The reconstructed ductal trees had Strahler number s=3 in nine cases (from eight women) and s=4 in two cases. We analyzed the R-matrices and performed classification of the autogalactograms for the nine ductal trees (extracted from eight women), with s=3.

The eight women (mean age 53.1 years; range 40-72 years) analyzed had four benign and one malignant radiological finding; three cases were normal. Table 1 lists patient's age at the exam, number of segmented image sets, number of MR slices with visible ductal segments per breast, and the type of reported findings. The listed cases were ordered by decreasing visibility of the ducts. The autogalactographic cases with reported normal, benign, or malignant radiological findings are labeled as "N", "B", or "M", respectively.

Table 1 List of MR autogalactograms. Provided are the patient's age at the time of the exam, the number of reconstructed ductal trees per patient, the number of MR slices with visible ductal segments per image set, and the findings from the radiology reports. The cases with reported normal, benign, or malignant radiological findings are labeled as "N", "B", or "M", respectively.

MRI Case #	Age	# of Trees	# of Slices with Ducts	Radiologic Findings
1	53	1	9	B
2	40	1	4	B
3	44	1	6	B
4	51	1	7	B
5	72	1	21	N
6	51	1	13	N
7	59	1	8	N
8	55	2	7	M

In our previous study, we analyzed 25 clinical x-ray galactograms obtained retrospectively from 15 women (mean age 49.2 years, range 29–75 years), examined at the Thomas Jefferson University Breast Imaging Center, Philadelphia, PA, during the period of June 1994 through January 2001. Of these, seven women (13 images) had radiological findings corresponding to benign abnormalities, and eight women (12 images) had no findings; no malignant cases were available. The patient's age at the time of the exam, the number of reconstructed trees per patient, and the reported radiologic findings are listed in Table 2.

Table 2 List of the x-ray galactographic cases, ordered by increasing patient's age at the exam. Listed are also the number of segmented images, and the type of corresponding radiological findings. (Cases with reported normal or benign findings are labeled "N" or "B", respectively).

X-ray Case #	Age	# of Images	Radiologic Findings
1	29	1	N
2	30	2	N
3	32	2	N
4	36	1	N
5	43	2	B
6	44	1	B
7	45	2	N
8	45	1	N
9	47	4 Images of 2 Trees	B
10	50	2	B
11	55	2	B
12	63	2	N
13	70	1	B
14	74	1	N
15	75	1	B

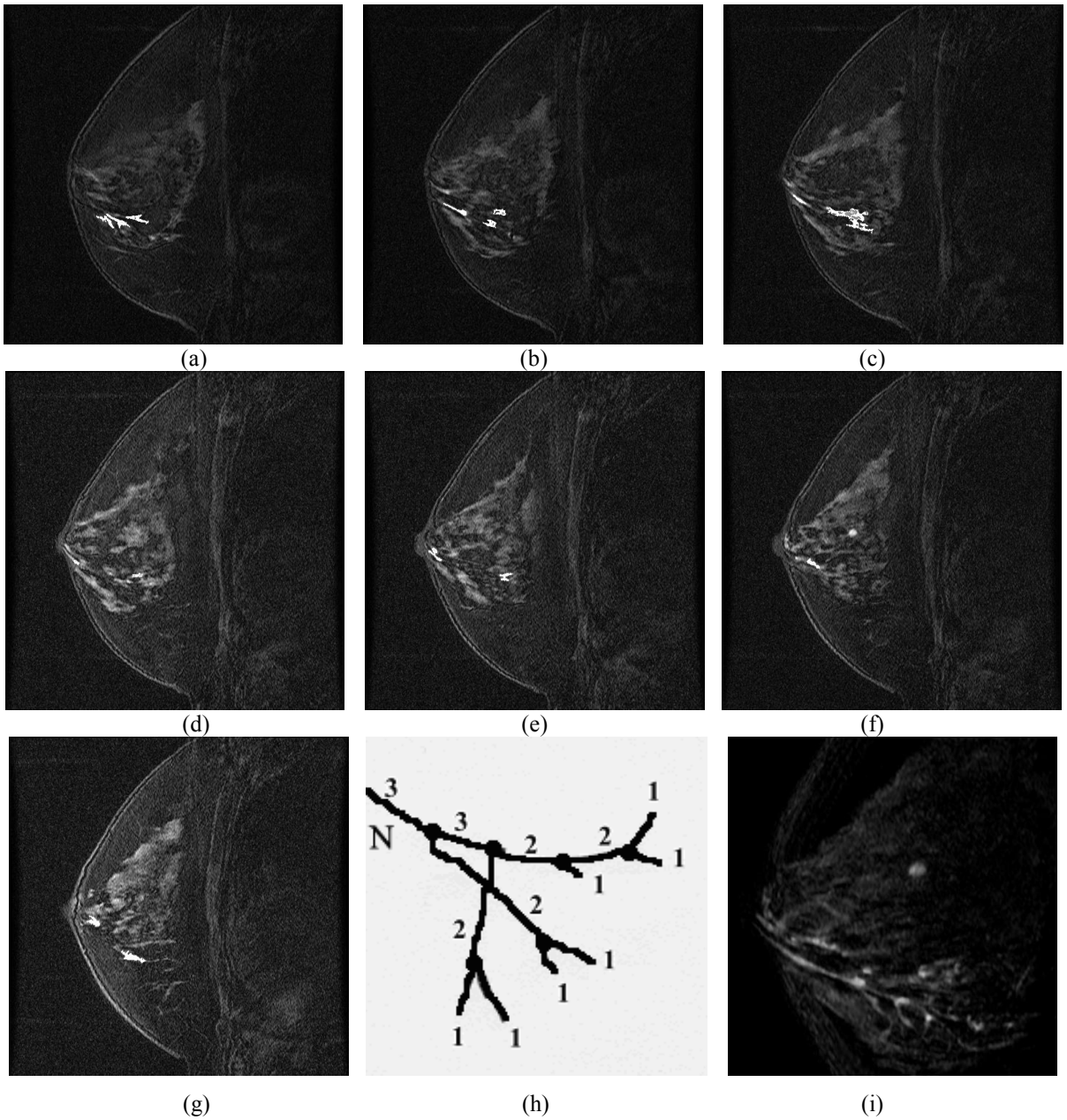

Figure 2: (a-g) Slices of the MR autogalactogram from clinical case #4, with the segmented ductal portions indicated in white. (h) A scan of the corresponding ductal tree, manually reconstructed based on the ductal segments. Tree branches are labeled for the purpose of computing R-matrix elements. ("N" indicates the position of the nipple.) (i) A volume rendering of the ductal branching network.

4. RESULTS

4.1 Results of duct segmentation and ductal tree reconstruction

Figure 2 shows the results of ductal segmentation of a MR autogalactogram, corresponding to case #4 from Table 1. Figure 2(a-g) shows individual MR slices with the ductal regions segmented using the region-growing method described in Section 2.1. Figure 2(h) shows the ductal tree reconstructed based on the segmented images from Figure 2(a-g). Figure 2(i) shows the case volume-rendered; the branching structure of the ductal tree is clearly visible. We used *JuliusLight* volume-rendering software (Research Center *CAESAR*, Bonn, Germany). The ramification matrix computed from the reconstructed tree shown in Figure 2(h), using the method described in Section 2.2, is given in Equation 2.

$$\mathbf{R} = \begin{bmatrix} 1/4 & 3/4 & . \\ 0 & 2/3 & 1/3 \end{bmatrix}. \tag{2}$$

4.2 MR autogalactogram classification results

The range of values of the classification feature, R-matrix element $r_{2,2}$, computed from six autogalactograms with radiological findings, MR_F+, and three autogalactograms without radiologic findings, MR_F-, are shown in Figure 3. In addition, Figure 3 shows the range of the galactogram classification feature, $r_{3,3}$, computed from 13 x-ray galactograms with, X-ray_F+, and 12 without radiologic findings, X-ray_F-.

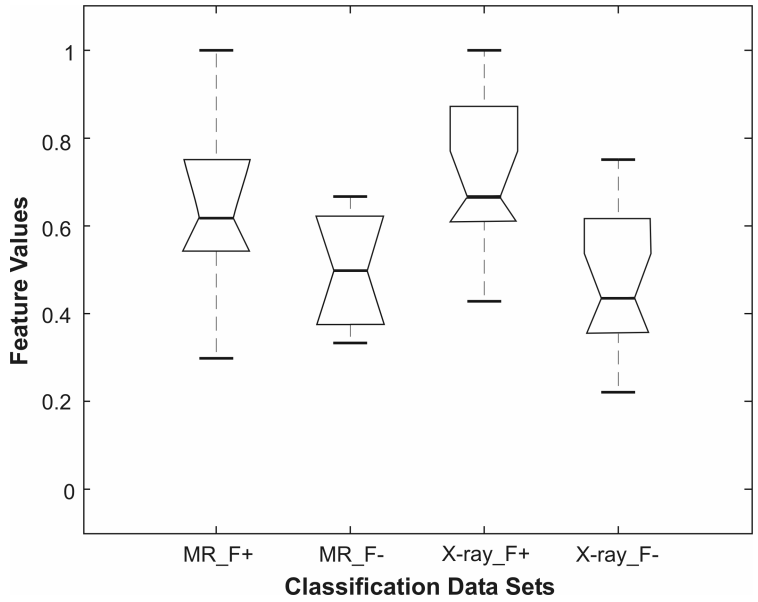

Figure 3: Box-whisker plots of feature values used for classification of MR autogalactograms and x-ray galactograms. The whiskers indicate maximum and minimum feature values and the box indicates 25-, 50-, and 75-percentile values. The notches represent an estimate of the uncertainty about the means, at the 5% significance level.

4.3 Comparison between performance of MR autogalactogram and x-ray galactogram classification

Figure 4 shows the ROC corresponding to the classification of individual image sets. The area under the ROC curve for the MR autogalactogram classification was equal to A=0.67, and the area under the ROC curve for the x-ray galactogram classification A=0.82.

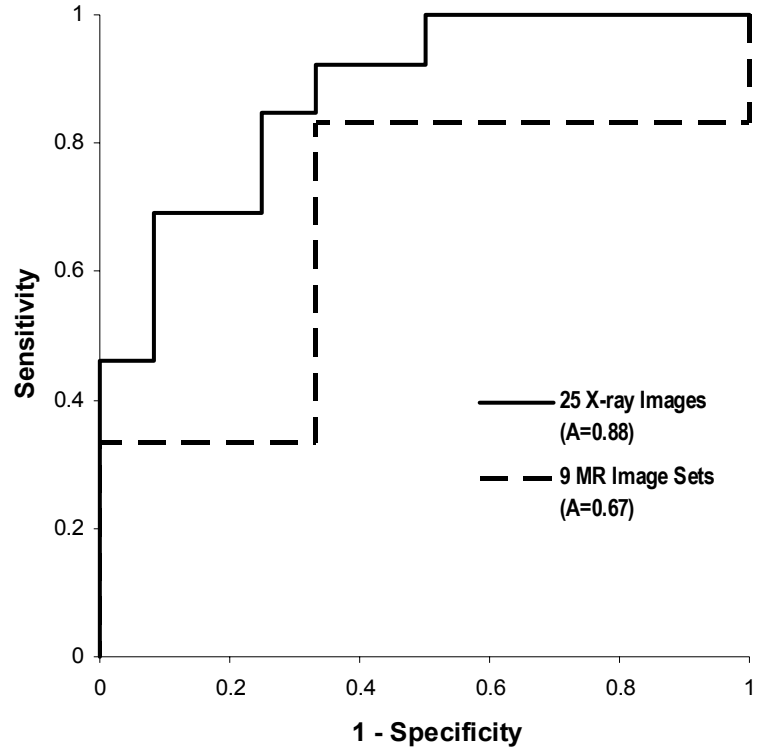

Figure 4: The ROC curves corresponding to the classification of individual data, MR autogalactographic image sets or x-ray galactographic images.

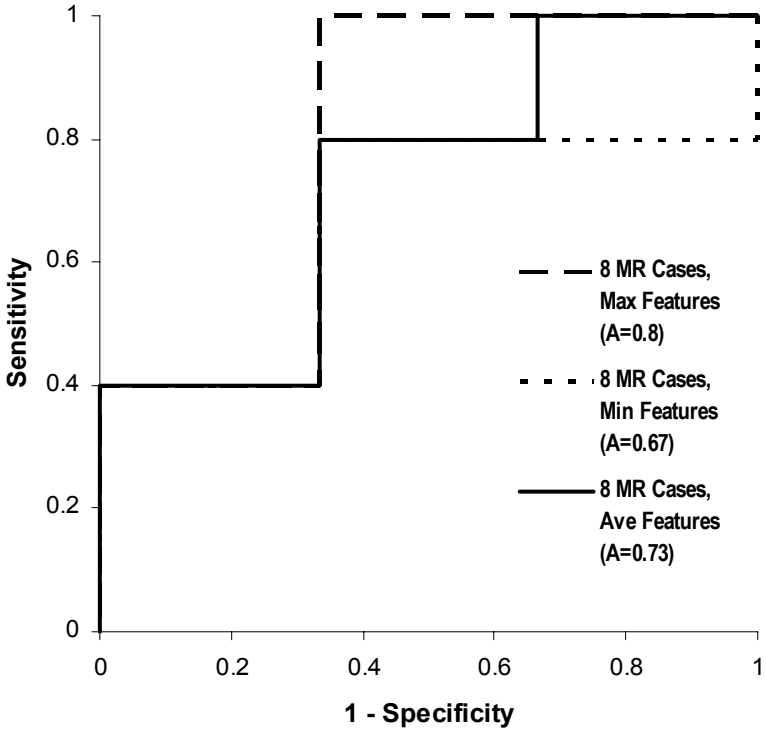

Figure 5: The ROC curves corresponding to the classification of patients based on their autogalactographic image sets. The radiologist's reports were used as the ground truth. Three different strategies for classifying cases with multiple image sets have been considered. The strategies correspond to assigning the maximum, minimum, or average feature value to each case.

Results of applying the three strategies for classification of patients with multiple images, described in Section 2.3, to the MR autogalactograms classification are shown in Figure 5. The values of the area under the ROC curve were equal to A=0.8, when using the maximum feature values, A=0.67, when using the minimum feature values, and A=0.73, when using the average feature values.

Similarly, results of the application of the three strategies for classifying x-ray galactography cases are shown in Figure 6. The values of the area under the ROC curve were equal A=0.86, when using the maximum feature values, A=0.82, when using the minimum feature values, and A=0.88, when using the average feature values.

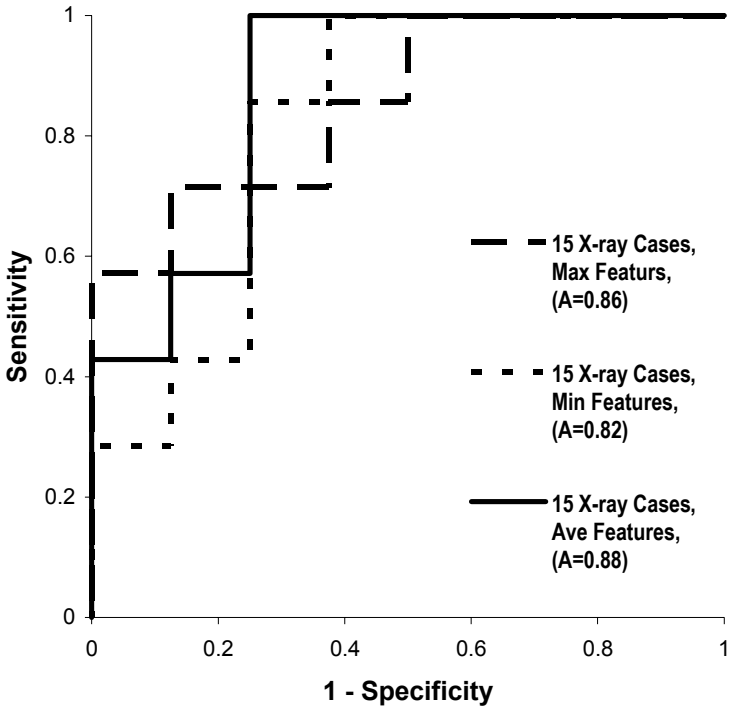

Figure 6: The ROC curves corresponding to the classification of patients based on their x-ray galactographic images, and the three strategies for classifying cases with multiple images, similar as in Figure 5.

Comparison between the case classification performances in the MR autogalactography and x-ray galactography studies has been shown in Figure 7, using the average feature values.

5. DISCUSSION AND CONCLUSIONS

To the best of our knowledge, the results presented here are the first report on the quantitative analysis of the 3D topological properties of breast ducts. These results, although derived from a small number of clinical cases, are supportive of our original findings from the analysis of x-ray galactograms. It appears that the performance of x-ray galactogram classification and MR autogalactogram classification are comparable. The analysis of the x-ray galactogram cases show higher classification accuracy (A=0.88) than for the MR autogalactograms (A=0.73), as shown in Figure 7. The x-ray study results show significant difference between the median feature values of the cases with and without radiological findings ($p<0.05$), as shown in Figure 3.

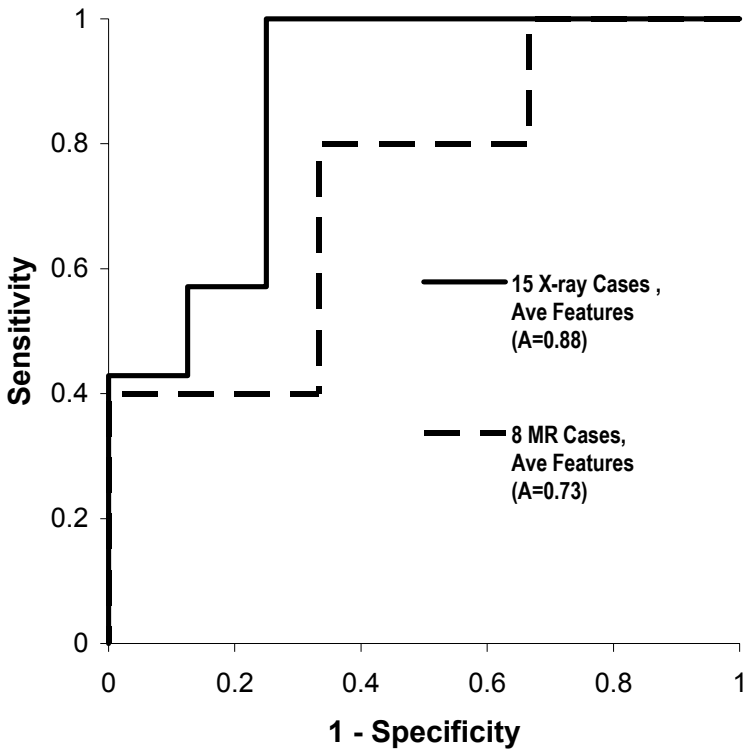

Figure 7: Comparison of the performances of classifying cases in the MR autogalactography and x-ray galactography studies. Cases with multiple images were classified using the average feature value from different images.

The MR results do not show statistical significance; however, they show a comparable trend. There are several reasons for this performance difference. First, the two studies differ in the number of visible ducts since MR imaging has a lower spatial resolution compared to x-ray galactography. In addition, x-ray galactograms have more uniform enhancement of the ductal network because an iodinated contrast agent is injected directly into ductal network, while in MR autogalactograms there is only partial enhancement of the ductal network. The selection of autogalactographic cases is also limited to women with proteinaceous/hemorrhagic ductal content.

The observed results provide anecdotal supporting evidence for the hypothesis that ductal morphology reflects breast disease status. We are currently planning further analysis, which include use of alternative 3D image acquisition modalities and development of an automated segmentation method. We are also considering alternative representations of the ductal tree topology. As the first step, we applied the string representation[20] to the data from our x-ray galactography study. The classification performance of the string representation based features was comparable with that of the R-matrix based features[21, 22].

ACKNOWLEDGMENT

The work was funded by Toshiba America Medical Systems Inc./Radiological Society of North America Research Seed Grant SD0329. The authors are grateful to Catherine Piccoli, M.D. and Andrea Frangos, M.S. from Thomas Jefferson University, Philadelphia, PA, for providing anonymized x-ray galactographic images, to Lubomir Hadjiiski, Ph.D. from University of Michigan, Ann Arbor, MI, for discussion about the classification of cases with multiple images, and to Vasileios Megalooikonomou, Ph.D. and Despina Kontos, M.S., from Temple University, Philadelphia, PA, for help with statistical analysis.

REFERENCES

1. Kopans D. *Breast Imaging*. Philadelphia, PA: Lippincott-Raven; 1998.
2. Lanyi M. *Diagnosis and differential diagnosis of breast calcifications*. Berlin, Germany: Springer-Verlag; 1988.
3. Bakic PR, Brzakovic D. Simulation of digital mammogram acquisition. Paper presented at: SPIE Medical Imaging, 1999; San Diego, CA.
4. Bakic PR, Albert M, Brzakovic D, Maidment ADA. Mammogram synthesis using a 3D simulation. I. Breast tissue model and image acquisition simulation. *Medical Physics.* 2002;29(9):2131-2139.
5. Bakic PR, Albert M, Brzakovic D, Maidment ADA. Mammogram synthesis using a 3D simulation. II. Evaluation of synthetic mammogram texture. *Medical Physics.* 2002;29(9):2140-2151.
6. Dance DR, Hunt RA, Bakic PR, et al. Breast dosimetry using high-resolution voxel phantoms. *Radiation Protection Dosimetry.* 2005;114:359-363.
7. Hunt RA, Dance DR, Bakic PR, et al. Calculation of the properties of digital mammograms using a computer simulation. *Radiation Protection Dosimetry.* 2005;114:395-398.
8. Richard FJP, Bakic PR, Maidment ADA. Mammogram registration: a phantom-based evaluation of compressed breast thickness variation effects. *IEEE Transaction of Medical Imaging.* 2006;25(2):188-197.
9. Hoeschen C, Tischenko O, Dance DR, Hunt RA, Bakic PR, Maidment ADA. Testing a wavelet based noise reduction method using computer simulated mammograms. Paper presented at: SPIE Medical Imaging, 2005; San Diego, CA.
10. Atwood CS, Hovey RC, Glover JP, et al. Progesterone induces side-branching of the ductal epithelium in the mammary glands of peripubertal mice. *Journal of Endocrinology.* 2000;167(1):39-52.
11. Bonta I, Giger M, Vyborny C, Heimann R, Li H, Mostardi P. Hot topic: Prognosis of breast cancer patients based on computerized mammographic analysis. Paper presented at: Radiological Society of North America Scientific Assembly and Annual Meeting, 2003; Chicago, IL.
12. Bakic PR, Albert M, Maidment ADA. Classification of galactograms with ramification matrices: Preliminary results. *Academic Radiology.* 2003;10(2):198-204.
13. Tabar L, Dean PB, Pentek Z. Galactography: the diagnostic procedure of choice for nipple discharge. *Radiology.* 1983;149(1):31-38.
14. Dinkel HP, Trusen A, Gassel AM, et al. Predictive value of galactographic patterns for benign and malignant neoplasms of the breast in patients with nipple discharge. *British Journal of Radiology.* 2000;73(871):706-714.
15. Viennot XG, Eyrolles N, Janey N, Arques D. Combinatorial analysis of ramified patterns and computer imagery of trees. *Comput Graph.* 1989;23:31-40.
16. Orel SG, Dougherty CS, Reynolds C, Czerniecki BJ, Siegelman ES, Schnall MD. MR imaging in patients with nipple discharge: Initial experience. *Radiology.* 2000;216:248-254.
17. Ibanez L, Schroeder W, Ng L, Cates J. *The ITK Software Guide*. 2 ed: Kitware, Inc.; 2005.
18. Efron B. *The jackknife, the bootstrap and other resampling plans.* Philadelphia, PA: SIAM; 1982.
19. Hanley JA, McNeil BJ. The meaning and use of the area under a receiver operating characteristic (ROC) curve. *Radiology.* 1982;143:29-36.
20. Chi Y, Yang Y, Muntz R. Canonical forms for labeled trees and their applications in frequent subtree mining. *Knowledge and information systems.* 2005;8:203-234.
21. Megalooikonomou V, Kontos D, Danglemaier J, Javadi A, Bakic PR, Maidment ADA. A representation and classification scheme for tree-like structures in medical images: An application on branching pattern analysis of ductal trees in x-ray galactograms. Paper presented at: SPIE Medical Imaging, 2006; San Diego, CA.
22. Kontos D, Megalooikonomou V, Javadi A, Bakic PR, Maidment ADA. Classification of galactograms using fractal properties of the breast ductal network. Paper presented at: IEEE International Symposium on Biomedical Imaging, 2006; Arlington, VA.